DIRECT NUMERICAL SIMULATION OF THE SPATIALLY DEVELOPING TURBULENT MIXING LAYER

I.C.C. de Bruin & B.J. Geurts
Faculty of Mathematical Sciences, University of Twente
P.O. Box 217, 7500 AE Enschede, The Netherlands

J.G.M. Kuerten
Department of Mechanical Engineering, Eindhoven University of Technology,
P.O. Box 513, 5600 MB Eindhoven, The Netherlands

ABSTRACT

A direct numerical simulation of transitional and developed turbulent flow in a three-dimensional spatially developing subsonic mixing layer is performed. The streamwise, normal and spanwise momenta are sampled at characteristic locations in the flow. The corresponding correlation time is computed in the turbulent regime and compared to the averaging time needed to obtain sufficiently accurate time-averaged flow quantities. Some resulting probability density functions are shown and discussed.

INTRODUCTION

We consider direct numerical simulations (DNS) of a subsonic spatially developing plane turbulent mixing layer. This flow can be used for a detailed investigation of the statistical properties in the turbulent regime. In this paper, we show the feasibility of present-day DNS for the study of statistical properties of spatially inhomogeneous turbulent flows. We first consider the required averaging time. A statistical analysis can be performed when the time-averaged solution is stationary. We therefore consider a criterion, based on the correlation time computed from the instantaneous solution, to derive the order of magnitude of the averaging time needed for a desired accuracy. This is illustrated with the time evolution of the averaged momentum and the momentum thickness.

Data is sampled from the instantaneous momenta in three directions. Several studies deal with the behaviour of probability density functions (*pdf*s) in homogeneous turbulence [10, 11, 12]. Most of these focus on *pdf*s of the velocity difference between two points separated by a certain distance and velocity derivative distributions. The focus in this paper is on *pdf*s of the three momenta for spatially inhomogeneous flow. The distribution in the turbulent regime turns out to approach Gaussian behaviour for the streamwise and spanwise momentum.

In the spatial setting that we employ, the computational domain is limited through the introduction of artificial boundaries. For the flow studied here, especially the outflow boundary requires some attention since no physical boundary condition is available in case of turbulent flow. A buffer domain is introduced in order to damp the reflections that may occur in the vicinity of the numerical outflow boundary. This procedure is combined with characteristic wave relations [7]. In the buffer domain, the turbulent solution which enters is gradually forced towards a steady mean flow near the end of the buffer. The damping function used here is formulated such that its effect is approximately grid independent and is found to be robust and with minimal upstream influence in both mixing- and boundary layer [1, 14].

We next introduce the numerical method and give a description of the flow. This is followed by the presentation of DNS results which are analysed and discussed. We focus on a criterion that prescribes the length of the time-interval needed in order to achieve a certain accuracy of the time-averaging procedure. We study the momentum thickness and the resulting growth rate. Probability density functions will be constructed from samples of the time evolution of momenta in all three directions. Finally some concluding remarks are collected.

NUMERICAL METHOD AND FLOW SETTING

A rectangular computational domain is used. An efficient spatial discretization which includes a fourth order finite volume technique suited for both uniform and stretched grids is employed. The time-integration uses a second order four-stage Runge-Kutta scheme [13].

The numerical method and boundary conditions are validated by imposing small perturbations on a base flow at the inflow boundary and comparing the results with Linear Stability Theory (LST) [1, 15]. The perturbations are composed of eigenfunctions corresponding to LST which provide a time dependent forcing of the flow at the inflow boundary. We observe a good agreement between the DNS and LST results, in particular if the resolution in the normal direction is adequate. Furthermore, it could be inferred that the upstream influence of the buffer domain is very small [1, 14].

In this paper we consider a mixing layer flow with a

Reynolds number of 200 and a Mach number of 0.8. The Reynolds number is based on the upper free-stream velocity, density and viscosity and half the vorticity thickness of the mean flow at the inflow while the Mach number is given by the ratio of the upper free stream velocity and speed of sound. We take a uniform grid in all directions. Considering previous results [14], we take a resolution of 25 points per perturbation wavelength of the most unstable LST mode in the streamwise and 128 points in the normal direction respectively. Furthermore, we take 16 points in the spanwise direction which extends half a spanwise wavelength using spanwise symmetry as described in [9]. This reduces the computer time and storage requirements by a factor of two.

In order to be able to reach transition to turbulence we use a streamwise extent of the computational domain of 18 perturbation wavelengths, of which the buffer length consists of two wave lengths. We observed no transition when only the most unstable fundamental 2D and 3D modes were used at the inflow, which shows the importance of the subharmonic modes. The pairing process was initiated after the inclusion of subharmonic modes. For transition to turbulence additional 3D modes were added. More details on the stages in the construction of this DNS can be found in [2]. In total the combination of the dominant 2D and 3D modes with their subharmonics at sufficient amplitude gives both a relatively simple and efficient inflow perturbation which is suitable for our purposes. The total amplitude of the perturbations imposed at the inflow is 0.2.

DNS RESULTS

In Figure 1 the spanwise vorticity is shown in a characteristic plane perpendicular to the spanwise direction at time 552. We can readily distinguish the different stages from laminar through transitional and turbulent flow. The time can be expressed in terms of the time needed for a signal to cross the streamwise domain, T_{tr}. This 'traversal' time scale is related to the average of the free stream velocities, and the length of the computational box. The time $T_0 = 552$ equals about 1.5 T_{tr} and from an investigation of the solution history at several characteristic locations in the flow it turned out to be a suitable starting moment of the time-averaging process. At this time the main initial transients have disappeared and a well developed time-dependent solution is obtained. Variations in the numerical parameters show the robustness of the physical predictions and justify the focus on the results arising from the DNS using LST perturbations [2, 3].

In order to perform a statistical study of the data, the streamwise momentum at nine different locations is sampled from $t = T_0$. We have chosen three stations in the streamwise direction, indicated by A, B and C respectively. As can be seen in Figure 1, the three streamwise locations are chosen in the laminar, transitional and turbulent regime respectively. For each location, we sample at three positions in the normal direction, located symmetrically around the centerline, and denoted by the subscripts l(ower), c(enterline) and u(pper).

TIME-AVERAGING

First, we study the length of the time interval needed for an accurate time-averaged solution. In numerical calculations as well as in physical experiments it is only possible to sample the solution over a finite time interval. The question is how long this time interval should be in order to achieve a certain accuracy, *i.e.* when can a finite-time average at any fixed location in the flow

$$\hat{u}_T = \frac{1}{T}\int_{T_0}^{T_0+T} u(t)dt$$

accurately approximate a statistical average. Here, we assume that the system is ergodic, so that the statistical average $\overline{u}$ equals the time average in the limit of infinite averaging time, *i.e.*

$$\overline{u} = \lim_{T\to\infty}\frac{1}{T}\int_{T_0}^{T_0+T} u(t)dt.$$

We start the averaging at $T_0 = 552$ since then the initialization transients have disappeared. Moreover, we checked that the results for higher values of T_0 are practically indistinguishable. Following [5] the relation between $\overline{u}$ and $\hat{u}_T$ is given by

$$\overline{|\hat{u}_T - \overline{u}|^2} \approx \frac{2\ T_{cor}\ b_{uu}(0)}{T} \qquad (1)$$

where an overbar denotes a statistical average and $b_{uu}(\tau)$ represents the Eulerian correlation function:

$$b_{uu}(\tau) = \overline{\Big(u(t+\tau)-\overline{u}\Big)\Big(u(t)-\overline{u}\Big)}.$$

Furthermore T_{cor} is the Eulerian correlation time defined as

$$T_{cor} = \frac{1}{b_{uu}(0)}\int_0^\infty b_{uu}(\tau)d\tau. \qquad (2)$$

In the results for the correlation function and correlation time we will show, we calculate the statistical averages by time averaging over the largest time interval available. Since these results are only used to get a crude estimate of the error in the time-averaged quantities this approximation appears allowed. For a reliable determination of the long time average $\overline{u}$, it is necessary to perform time-averaging over a period T much larger than the correlation time T_{cor}. We may use relation (1) to estimate the necessary averaging time T in terms of units T_{cor} and a desired level of accuracy for $|\hat{u}_T - \overline{u}|^2$.

In Figure 2 we plotted the correlation functions $b_{uu}(\tau)$ based on the streamwise momentum obtained from the time interval [1.5 T_{tr}, 9 T_{tr}]) for the three locations of station C. The correlation functions display the characteristic behaviour of a fast decay to zero followed by oscillations. Due to these oscillations the correlation time defined by (2) is hard to calculate. In

practice the correlation time is often calculated by integrating the correlation function until its first root. This results in $T_{cor} \approx 6$ for the lower and ≈ 7 for the centerline and upper location. The correlation time appears to vary somewhat in the turbulent regime. Using relation (1) we estimate that the averaging time should be about 1000 time units for an absolute error in $\overline{u}$ of 1% $\left(\text{implying } \overline{|\hat{u}_T - \overline{u}|^2} = 1 \cdot 10^{-4}\right)$ and about 4000 time units for an error of 0.5%.

In order to check the approximation of the averaging time derived above, we plot the time-averaged streamwise momentum $\hat{u}_T$ as a function of the averaging time T in Figure 3 for the centerline location in the turbulent regime. This average corresponds to the instantaneous signal part of which is shown in Figure 4. We note the long term oscillation that is present in Figure 3 as a result of the incorporation of modes with nearly the same frequencies at the inflow. It can be inferred that after about 1000 time units ($\approx 2.5\ T_{tr}$) the deviation is within 1%. Finally, we mention that the general decrease of $\hat{u}_T - \overline{u}$ behaves as the square root of T corresponding to the behaviour predicted by relation (1). After this focus on the time-averaging process, we continue with a study of the momentum thickness based on the averaged solution. The probability density functions for the instantaneous momenta in all directions are computed and some characteristic features will be considered.

MOMENTUM THICKNESS

The momentum thickness θ is an integral variable based on the averaged solution [8]. The momentum thickness appears in good approximation to be a linear function of the streamwise coordinate in a large part of the domain. This makes it a suitable variable in the study of similarity of the flow in the turbulent regime where it can be used for the scaling of the normal coordinate in order to study *e.g.* the time-averaged Reynolds stress [2].

For the approximation of the growth rate $\alpha = d\theta/dx_1$ we use the method of least squares fit in the appropriate part of the domain. Other alternatives are available and give rise to the same conclusions. The estimate of α depends slightly on the location and length of the streamwise domain used for its determination, as well as on the length of the time interval used for computation of the average solution. However, with suitably long time integration an accurate estimate can be obtained as above.

In Figure 5 the momentum thickness, averaged over about 7.5 T_{tr} and the spanwise direction, is plotted as a function of the streamwise coordinate. The computed thickness can be compared with the thickness of the laminar field which is proportional to the square root of the streamwise coordinate. Because the solution is damped to the laminar solution at the end of the buffer, it is clear that both lines coincide near the inflow as well as the outflow boundary. The results presented do not change significantly when the averaging is started at a later moment in time *e.g.* 2 T_{tr} instead of 1.5 T_{tr}. Interpreting the data from Figure 5, the resulting growth rate equals 0.0138. From [4], for incompressible shear layers with equal freestream densities, the momentum thickness growth rate was found to be in the range [0.010,0.019]. The value computed here falls well in this range.

PROBABILITY DENSITY FUNCTIONS

The solution is recorded for 7.5 T_{tr}, resulting in about 21500 data points for each location. As an illustration, in Figure 4, part of the history in time is shown for the streamwise momentum at the centerline of station C in the turbulent regime. From this kind of data the probability density functions (*pdf*) are plotted in Figure 6. For each *pdf* the value-range is divided into 12 equally long intervals. This number was found appropriate for the generation of the *pdf*s. The shape of the *pdf* at the upstream location reflects the gradual change of the inflow distribution into a turbulent distribution. For all three locations in the turbulent regime (Figure 6c) the *pdf*s are quite close to a Gaussian distribution at the same mean and standard deviation. In addition, the *pdf*s at locations C_l and C_u display a characteristic asymmetry. The *pdf* of the velocity fluctuations in homogeneous turbulence is often assumed to be Gaussian. Experimental results show this and differences are usually attributed to experimental uncertainty [10]. The deviations from a Gaussian distribution can be quantified by considering the so-called skewness and flatness [5]. These quantities, including the standard deviation, are shown in Table 1 for the three momenta at the three locations in the turbulent regime. The values for the streamwise momentum skewness illustrate the asymmetry mentioned above and the flatness values are close to 3.0, the equivalent for a random variable with Gaussian distribution.

The *pdf*s for the normal and spanwise momentum in the turbulent regime are shown in Figure 7. The normal momentum *pdf* in Figure 7a displays an equivalent but stronger skewness on both sides of the center line compared to the streamwise momentum *pdf* in Figure 6c. This is illustrated quantitatively in Table 1. The mean values are about $8.7\ 10^{-3}, 1.8\ 10^{-3}$ and $-5.8\ 10^{-3}$ for the low speed, centerline and high speed side respectively. This decrease of the normal momentum when moving upwards corresponds with the fact that fluid from the far field is moving towards the kernel of the mixing layer. Comparison with the spanwise momentum *pdf* in Figure 7c and Table 1 reveals a larger standard deviation for the normal momentum. In contrast to both the streamwise and normal momenta, the spanwise momentum distribution is about similar at all three locations. It appears almost symmetric around zero with the smallest standard deviation at the high velocity side. This is explained by the fact that the mixing layer is bending down slightly to the low-speed

side [6] resulting in a high-speed side containing less turbulence. Furthermore the spanwise momentum *pdf* is close to a Gaussian distribution. Finally, we mention that the values presented in Table 1 and the *pdf*s in Figures 6 and 7 are based on the same data. Comparison with data from a shorter time interval reveals that the values of Table 1 have converged.

CONCLUSION

We have described DNS results of a turbulent mixing layer. A statistically stationary state was reached and sampled. The correlation time was computed and related to the length of the time interval in the time-averaging in order to achieve a certain accuracy. This was illustrated with the convergence of the streamwise averaged momentum. Furthermore the momentum thickness displayed a linear growth in the streamwise direction. An extensive study of the distribution of the velocities at several locations was performed. The *pdf* approached the Gaussian distribution for the streamwise and spanwise momenta at the turbulent location far downstream. The results encourage the application of the numerical method to Large-Eddy simulations and analysis of terms arising in the Reynolds-averaged Navier-Stokes equations which will be considered in the nearby future.

References

[1] de Bruin I.C.C., Wasistho B., Geurts B.J., Kuerten J.G.M. & P.J. Zandbergen, Simulation of Subsonic Spatially Developing Turbulent Shear Flows, *Proceedings XVIth ICNMFD*, France, 1998.

[2] de Bruin I.C.C., Geurts B.J., & Kuerten J.G.M., DNS evidence of Self-similar Flow in a Spatially Developing Turbulent Mixing Layer, *in preparation*, 1999.

[3] de Bruin I.C.C., Geurts B.J., Kuerten J.G.M. & Driesen C.H., Robustness of flow phenomena in a spatially developing turbulent mixing layer, *Proc. 2nd AFOSR conference on DNS & LES,* 1999.

[4] Dimotakis P.E., Turbulent Free Shear Layer Mixing and Combustion, *Progress in Astronautics and Aeronautics,* 137, pp. 265-340, 1991.

[5] Monin A.S. & Yaglom A.M., *Statistical Fluid Mechanics*, Mechanics of Turbulence Volume 1, MIT Press, Cambridge, 1977.

[6] Oster D. & Wygnanski I., The forced mixing layer between parallel streams, *J. Fluid Mech.*, 123, pp. 91-130, 1982.

[7] Poinsot T.J. & Lele S.K., Boundary Conditions for Direct Simulations of Compressible Viscous Flows, *J. of Comp. Phys.*, 101, pp. 104-129, 1992.

[8] Ragab S.A. & Sheen S., The nonlinear development of supersonic instability waves in a mixing layer, *Phys. Fluids A*, 4(3), pp. 553-566, 1992.

[9] Sandham N. & Kleiser L., The late stages of transition to turbulence in channel flow, *J. Fluid Mech.,* 245, pp. 319-348, 1992.

[10] Screenivasan K.R. & Antonia R.A., The phenomenology of small-scale turbulence, *Annu. Rev. Fluid Mech.*, 29, pp. 435-472, 1997.

[11] Tavoularis S. & Corrsin S., Experiments in nearly homogenous turbulent shear flow with a uniform mean temperature gradient, *J. Fluid Mech.,* 104, pp. 311-347, 1981.

[12] Vincent A. & Meneguzzi M., The spatial structure and statistical properties of homogeneous turbulence, *J. Fluid Mech.*, 225, pp. 1-20, 1991.

[13] Vreman B., Geurts B.J. & Kuerten J.G.M., Large-Eddy Simulation of the Turbulent Mixing Layer, *J. Fluid Mech.*, 339, pp. 357-390, 1997.

[14] Wasistho B., Geurts B.J. & Kuerten J.G.M., Simulation techniques for spatially evolving instabilities in compressible flow over a flat plate, *Computers and Fluids*, 26, pp. 713-739, 1997.

[15] Wasistho B., de Bruin I.C.C., Geurts B.J. & Kuerten J.G.M., Direct Numerical Simulation of Subsonic Spatially Developing Shear Flows, *Advances in Turbulence VII,* pp. 175-178, Kluwer Academic Publishers, 1998.

	σ ($\cdot 0.01$)			s			δ		
	ρu_1	ρu_2	ρu_3	ρu_1	ρu_2	ρu_3	ρu_1	ρu_2	ρu_3
u(upper)	6.8	7.4	6.6	-0.54	0.64	-0.30	3.0	3.0	3.3
c(enterline)	7.0	8.2	7.6	-0.11	0.049	-0.23	2.7	3.3	2.7
l(ower)	6.5	7.5	7.1	0.31	0.49	0.11	2.9	2.9	3.0

Table 1: Standard deviation (σ), skewness (s) and flatness (δ) of the *pdf*s (plotted in Figures 6c and 7 respectively) for the three locations at the turbulent station C.

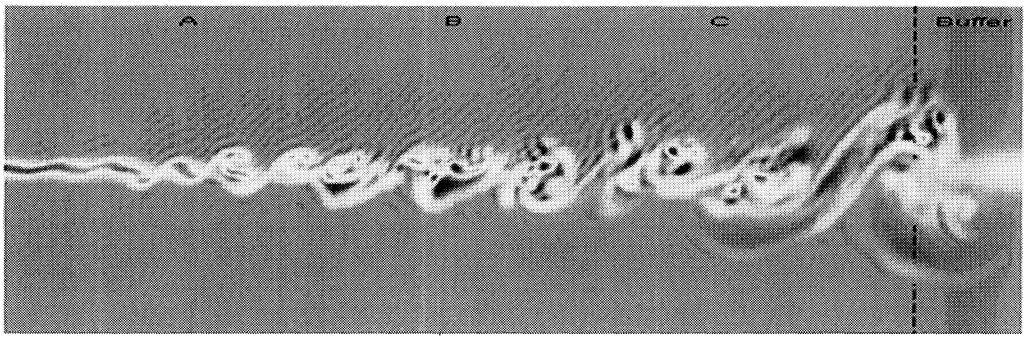

Figure 1: Contourplot of the spanwise vorticity in a spanwise plane. The streamwise extent consists of 16 perturbation wavelengths of the linearly dominant 2D mode in the physical domain and 2 perturbation wavelengths in the buffer.

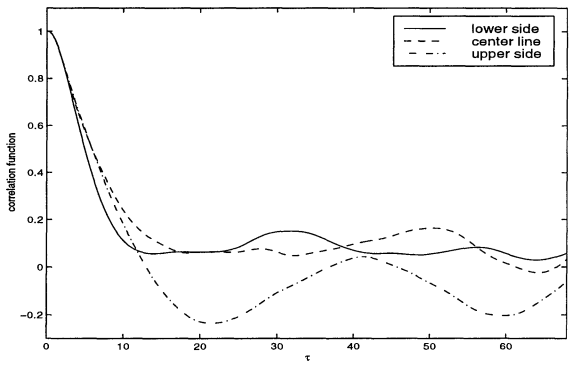

Figure 2: Normalized correlation functions of ρu_1 at station C (turbulent regime).

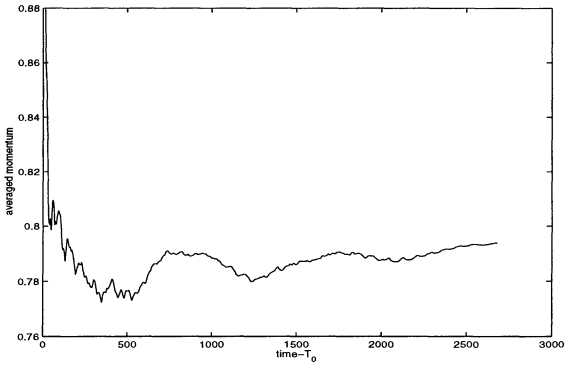

Figure 3: Averaged streamwise momentum at location C_c.

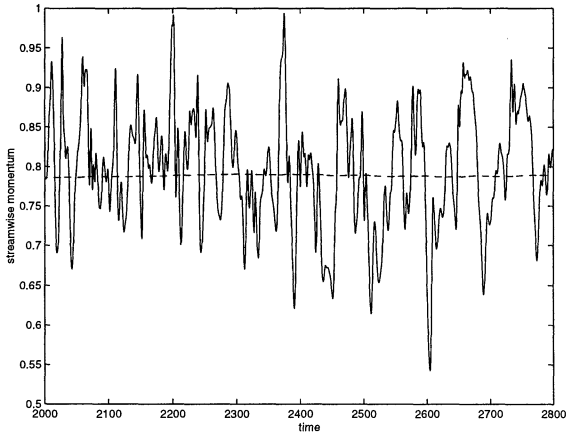

Figure 4: Streamwise momentum at station C_c and its average (dashed).

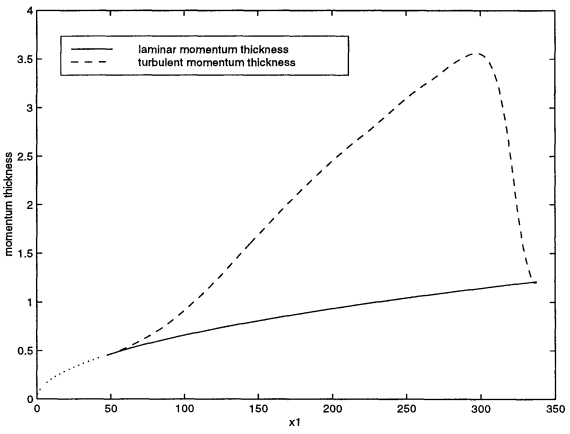

Figure 5: Momentum thickness as a function of the streamwise coordinate.

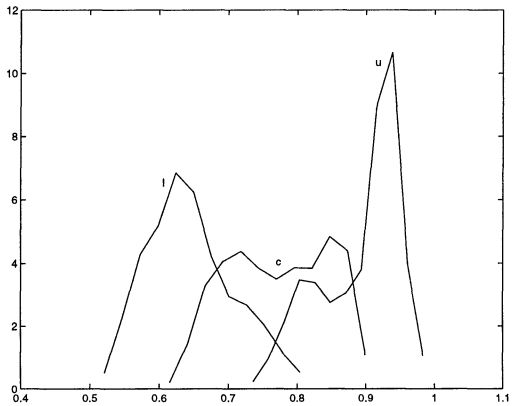

a: *pdf* ρu_1 at station A.

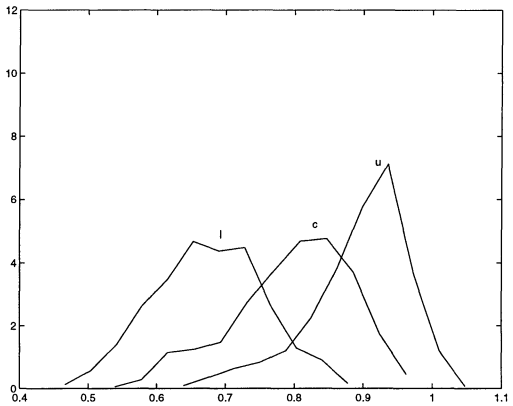

b: *pdf* ρu_1 at station B.

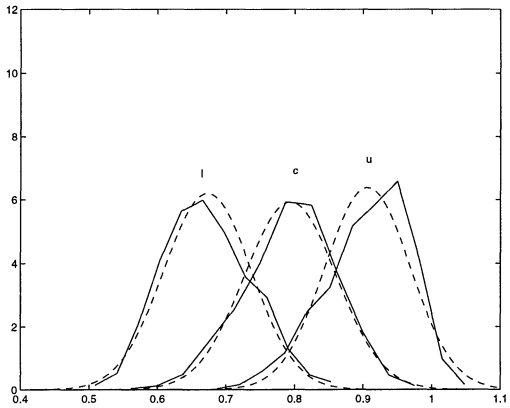

c: *pdf* ρu_1 at station C.

Figure 6: Probability density functions of the streamwise momentum. The corresponding Gaussian distributions are included as well (dashed) at station C.

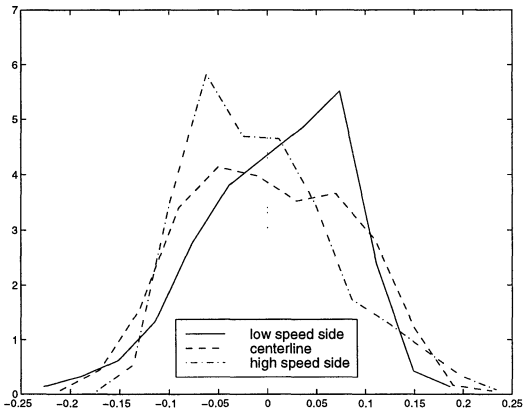

a: Normal momentum *pdf*

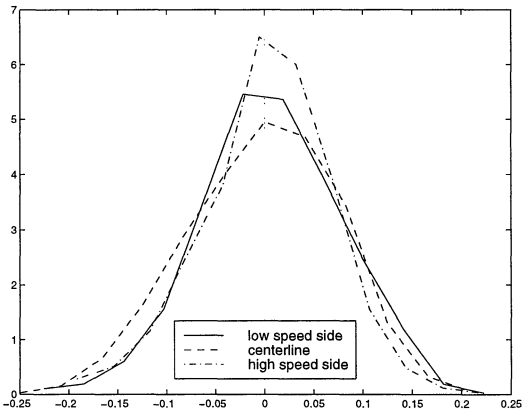

b: Spanwise momentum *pdf*

Figure 7: Probability density functions of the normal and spanwise momenta at the 3 locations of station C.